The Journal of Chemical Physics

Static field-gradient polarizabilities of small atoms and molecules at finite temperature

Cite as: J. Chem. Phys. **147**, 204101 (2017); https://doi.org/10.1063/1.4999840
Submitted: 11 August 2017 . Accepted: 06 November 2017 . Published Online: 22 November 2017

Juha Tiihonen, Ilkka Kylänpää, and Tapio T. Rantala

Static field-gradient polarizabilities of small atoms and molecules at finite temperature

Juha Tiihonen,[a] Ilkka Kylänpää,[b] and Tapio T. Rantala
Laboratory of Physics, Tampere University of Technology, P.O. Box 692, FI-33101 Tampere, Finland

(Received 11 August 2017; accepted 6 November 2017; published online 22 November 2017)

In this work, we propose new field-free estimators of static field-gradient polarizabilities for finite temperature path-integral Monte Carlo method. Namely, dipole–quadrupole polarizability A, dipole–dipole–quadrupole polarizability B, and quadrupole–quadrupole polarizability C are computed for several up to two-electron systems: H, H^-, He, Li^+, Be^{2+}, Ps_2, PsH, H_2^+, H_2, H_3^+, and HeH^+. We provide complementary data for ground state electronic properties within the adiabatic approximation and demonstrate good agreement with available values in the literature. More importantly, we present fully non-adiabatic results from 50 K to 1600 K, which allow us to analyze and discuss strong thermal coupling and rovibrational effects in total field-gradient polarizabilities. These phenomena are most relevant but clearly overlooked, e.g., in the construction of modern polarizable force field models. However, our main purpose is demonstrating the accuracy and simplicity of our approach in a problem that is generally challenging. *Published by AIP Publishing.* https://doi.org/10.1063/1.4999840

I. INTRODUCTION

Computation of the electric field response at quantum mechanical level—polarizability—is a fundamental problem in electronic structure theory. Approaching it from the first-principles is challenging but well motivated: polarizabilities have implications in many physical properties and modeling aspects, such as optical response and atomic and molecular interactions. Method development and understanding of polarizability has been vast over the past several decades, but the main focus has always been on the bare ground state properties.[1–3] While the finite temperature regime is formally well established,[4] explicit results beyond the Born–Oppenheimer approximation are scarce. By introducing efficient polarizability estimators for the finite temperature path-integral Monte Carlo (PIMC) method, we are aiming to change that.

In our recent article,[5] we proposed a scheme for estimating static dipole polarizabilities in a field-free PIMC simulation. This was an improvement to our earlier finite-field approach.[6] The resulting properties, including substantial rovibrational effects, were those corresponding to an isolated molecule in low density gas. However, the dipole-induced polarizabilities only describe the effects of a uniform electric field.

In this work, we complement our tools by introducing similar estimators for the field-gradient polarizabilities. According to the definitions of Buckingham,[1] the foremost properties are dipole–quadrupole polarizability A, dipole–dipole–quadrupole polarizability B, and quadrupole–quadrupole polarizability C. As the names suggest, they have a direct consequence in treating the long-range interactions between atoms or molecules. There is emerging interest in polarizable force field models[7,8] and van der Waals coefficient formulae[9] employing polarizabilities of all orders. However, the employed properties are often only electronic averages or fully empirical fits, while rovibrational coupling is completely overlooked. Here, we show that finite temperature has an immense effect on total molecular field-gradient polarizabilities.

At first, we present the analytic forms of the field-free PIMC estimators. After this, we demonstrate their capability in a series of simulations for different small atoms, ions, and molecules. The results are compared against values available in the literature. However, to the best of our knowledge, many of them are presented here for the first time. This is most pronounced in the non-adiabatic simulations, which include all rovibrational and electronic effects at finite temperature.

II. THEORY

Let us consider a system of N distinguishable particles in coordinate-space R and at inverse temperature $\beta = \hbar/k_B T$. Later, $\hbar = 1$. The thermal density matrix $\rho(R, R'; \beta)$ is given by the density operator

$$\rho(R, R'; \beta) = \langle R|\hat{\rho}(\beta)|R'\rangle, \tag{1}$$

where $\hat{\rho}$ is also identified as a retarded propagator in imaginary-time,

$$\hat{\rho}(\beta) = e^{-\beta\hat{H}} = e^{-i(t-t_0)\hat{H}} = \hat{G}(t - t_0), \tag{2}$$

where $i(t - t_0) = \beta = 1/k_B T$.

[a]tiihonen@iki.fi
[b]Present address: Materials Science and Technology Division, Oak Ridge National Laboratory, Oak Ridge, Tennessee 37831, USA.

A. Perturbation of properties

The expectation value $\langle O\rangle$ of a property $\hat{O}$ is given by a weighted trace of the density matrix

$$\begin{aligned}\langle O\rangle &= Z^{-1}\int dR\left\langle R\left|\hat{O}\hat{\rho}(\beta)\right|R\right\rangle \\ &= Z^{-1}\int dRdR'\left\langle R\left|\hat{O}\right|R'\right\rangle\langle R'|\hat{\rho}(\beta)|R\rangle,\end{aligned} \tag{3}$$

where

$$Z = \int dR\langle R|\hat{\rho}(\beta)|R\rangle \tag{4}$$

is the partition function. If $\hat{O}$ is diagonal, then

$$\int dR'\left\langle R\left|\hat{O}\right|R'\right\rangle = \int dR'\langle R|R'\rangle O(R') = O(R) \tag{5}$$

and Eq. (3) simplifies to

$$\langle O\rangle = Z^{-1}\int dRO(R)\rho(R,R;\beta). \tag{6}$$

Now, consider a perturbation λ_1. The response of $\hat{O}$ with respect to this perturbation is given to the first order by a differential of Eq. (3),

$$\begin{aligned}\frac{\partial}{\partial\lambda_1}\langle O\rangle &= \frac{\partial}{\partial\lambda_1}Z^{-1}\int dR\left\langle R\left|\hat{O}\hat{\rho}(\beta)\right|R\right\rangle \\ &= Z^{-1}\int dR\left\langle R\left|\hat{O}\frac{\partial}{\partial\lambda_1}\hat{\rho}(\beta)\right|R\right\rangle \\ &\quad - Z^{-2}\int dR\left\langle R\left|\hat{O}\hat{\rho}(\beta)\right|R\right\rangle\int dR\left\langle R\left|\frac{\partial}{\partial\lambda_1}\hat{\rho}(\beta)\right|R\right\rangle \\ &= \left\langle O\frac{\partial\rho}{\partial\lambda_1}\right\rangle - \langle O\rangle\left\langle\frac{\partial\rho}{\partial\lambda_1}\right\rangle,\end{aligned} \tag{7}$$

where we have used the Hellman–Feynman theorem and assumed no dependence between λ and $\hat{O}$ or $|R\rangle$. The higher order responses, i.e., differentials of the form $\frac{\partial}{\partial\lambda_1}\frac{\partial}{\partial\lambda_2}\ldots$ can be easily derived similar to Eq. (7). In particular, the second order is given by

$$\begin{aligned}\frac{\partial}{\partial\lambda_1}\frac{\partial}{\partial\lambda_2}\langle O\rangle &= \frac{\partial}{\partial\lambda_1}\left[\left\langle O\frac{\partial\rho}{\partial\lambda_2}\right\rangle - \langle O\rangle\left\langle\frac{\partial\rho}{\partial\lambda_2}\right\rangle\right] \\ &= \left\langle O\frac{\partial\rho}{\partial\lambda_2}\frac{\partial\rho}{\partial\lambda_1}\right\rangle - \left\langle\frac{\partial\rho}{\partial\lambda_1}\right\rangle\left\langle\frac{\partial\rho}{\partial\lambda_2}O\right\rangle \\ &\quad - \left\langle O\frac{\partial\rho}{\partial\lambda_1}\right\rangle\left\langle\frac{\partial\rho}{\partial\lambda_2}\right\rangle - \langle O\rangle\left\langle\frac{\partial\rho}{\partial\lambda_2}\frac{\partial\rho}{\partial\lambda_1}\right\rangle \\ &\quad + 2\langle O\rangle\left\langle\frac{\partial\rho}{\partial\lambda_2}\right\rangle\left\langle\frac{\partial\rho}{\partial\lambda_1}\right\rangle,\end{aligned} \tag{8}$$

and so on. Clearly, the calculation of the response boils down to the differential of the density operator. Using the exact density matrix from Eqs. (1) and (2), the derivative is given by

$$\frac{\partial}{\partial\lambda_1}\hat{\rho}(\beta) = \beta\hat{\rho}(\beta)\left(-\frac{\partial\hat{H}}{\partial\lambda_1}\right). \tag{9}$$

However, in practical calculations, the exact density matrix is rarely available. Therefore, it becomes necessary to approximate $\hat{\rho}(\beta)$ by dividing it to small intervals. That is, we consider $\hat{\rho}(\tau)$, where $\tau = \beta/M$ and M is an arbitrary large integer. Based on the properties of Green's functions,[11] we may then rewrite the propagator from R to R' as

$$\langle R|\hat{\rho}(\beta)|R'\rangle = \prod_{i=0}^{M-1}\langle R_i|\hat{\rho}(\tau)|R_{i+1}\rangle, \tag{10}$$

where $R_0 = R$ and $R_M = R'$ and whose full phase-space path-integral is written as $\int dR_1\ldots dR_M$. The differential of Eq. (10) is now given by

$$\begin{aligned}\frac{\partial}{\partial\lambda_1}\prod_{i=0}^{M-1}\langle R_i|\hat{\rho}(\tau)|R_{i+1}\rangle &= \sum_{j=1}^{M}\prod_{i=0,i\neq j}^{M-1}\left\langle R_j\left|\frac{\partial}{\partial\lambda_1}\hat{\rho}(\tau)\right|R_{j+1}\right\rangle \\ &\quad\times\langle R_i|\hat{\rho}(\tau)|R_{i+1}\rangle \\ &= \sum_{j=1}^{M}\prod_{i=0,i\neq j}^{M-1}\left\langle R_j\left|\tau\hat{\rho}(\tau)\left(-\frac{\partial\hat{H}}{\partial\lambda_1}\right)\right|R_{j+1}\right\rangle \\ &\quad\times\langle R_i|\hat{\rho}(\tau)|R_{i+1}\rangle \\ &= \frac{\beta}{M}\sum_{j=1}^{M}\prod_{i=0,i\neq j}^{M-1}\left\langle R_j\left|\hat{\rho}(\tau)\hat{D}_1\right|R_{j+1}\right\rangle \\ &\quad\times\langle R_i|\hat{\rho}(\tau)|R_{i+1}\rangle,\end{aligned} \tag{11}$$

where $\hat{D}_1 = -\frac{\partial\hat{H}}{\partial\lambda_1}$. If $\hat{D}_1$ is a diagonal operator, we may use Eq. (5) such that under the path-integration, each time-slice yields $\int dR_{j+1}\langle R_j|\hat{D}|R_{j+1}\rangle = O(R_j)$. This allows us to express the expectation value of the derivative as

$$\begin{aligned}\left\langle\frac{\partial\hat{\rho}(\beta)}{\partial\lambda_1}\right\rangle &= \frac{\beta}{M}\sum_{j=0}^{M-1}\int dR_1\ldots dR_M\prod_{i=1}^{M}\rho(R_{i-1},R_i;\tau)D_1(R_j) \\ &= \beta\left\langle\bar{D}_1(\beta)\right\rangle,\end{aligned} \tag{12}$$

where $\bar{D}_1(\beta)$ means the average over a sample path with the total length of $M\tau = \beta$. It is important to appreciate this property: for a discrete sample path, the correct result can only be obtained by taking the average over all time-slices rather than measuring just one. In fact, the latter is only possible, when $\hat{D}_1$ commutes with $\hat{\rho}$ (that is, $\hat{H}$), but even then using the average is more efficient in a practical implementation. Finally, we note that the result of Eq. (12) can be generalized to the product of multiple derivatives (and, optionally, a diagonal observable $\hat{O}$) such that

$$\left\langle\frac{\partial\hat{\rho}(\beta)}{\partial\lambda_1}\cdots\frac{\partial\hat{\rho}(\beta)}{\partial\lambda_L}\hat{O}\right\rangle = \beta^L\left\langle\bar{D}_1(\beta)\ldots\bar{D}_L(\beta)\bar{O}(\beta)\right\rangle, \tag{13}$$

as long as $\hat{O}$ and all of the $\hat{D}$ commute with each other. For convenience and efficiency, the path-average property has been applied to $\hat{O}$ also. This can be done when the density matrix is symmetric in the phase-space and imaginary-time.[11]

B. Field-gradient polarizabilities

Now, let us consider higher order responses to the electric field, that is, polarizabilities. Let $H^{(0)}$ be the unperturbed many-body Hamiltonian with full interactions. A perturbation caused by a uniform external electric field F_α and the field-gradient $F_{\alpha\beta} = (\nabla F_\alpha)_\beta$ gives the total Hamiltonian as

$$\hat{H}^{(1)} = \hat{H}^{(0)} - \hat{\mu}_\alpha F_\alpha - \tfrac{1}{3}\hat{\Theta}_{\alpha\beta}F_{\alpha\beta} - \cdots, \tag{14}$$

where $\hat{\mu}_\alpha$ and $\hat{\Theta}_{\alpha\beta}$ are the dipole and (traceless) quadrupole moment operators, respectively. Indices α, β, γ, δ, ... refer to the Einstein summation of the combinations of x, y, and z. According to the Buckingham convention,[1] the change in total energy is written as a perturbation expansion of coefficients

$$\begin{aligned} E^{(1)} = E^{(0)} &- \mu_\alpha F_\alpha - \frac{1}{2}\alpha_{\alpha\beta}F_\alpha F_\beta - \frac{1}{6}\beta_{\alpha\beta\gamma}F_\alpha F_\beta F_\gamma \\ &- \frac{1}{24}\gamma_{\alpha\beta\gamma\delta}F_\alpha F_\beta F_\gamma F_\delta - \frac{1}{3}\Theta_{\alpha\beta}F_{\alpha\beta} \\ &- \frac{1}{3}A_{\gamma,\alpha\beta}F_\gamma F_{\alpha\beta} - \frac{1}{6}B_{\alpha\beta,\gamma\delta}F_\alpha F_\beta F_{\gamma\delta} \\ &- \frac{1}{6}C_{\alpha\beta,\gamma\delta}F_{\alpha\beta}F_{\gamma\delta} - \cdots . \end{aligned} \tag{15}$$

Here, μ_α and $\Theta_{\alpha\beta}$ are the permanent dipole and quadrupole moments, respectively. Coefficients α, β, and γ are static dipole polarizabilities of different orders. They have been treated earlier.[5] In this work, we focus on the field-gradient polarizabilities A, B, and C, which are called dipole–quadrupole, dipole–dipole–quadrupole, and quadrupole–quadrupole polarizabilities, respectively.

We can solve for the individual properties by differentiating Eq. (15) with respect to the perturbation in the zero-field limit. In particular, we get

$$A_{\alpha,\beta\gamma} = -3\lim_{F\to 0}\frac{\partial}{\partial F_{\beta\gamma}}\frac{\partial}{\partial F_\alpha}E^{(1)} = 3\lim_{F\to 0}\frac{\partial}{\partial F_{\beta\gamma}}\mu_\alpha, \tag{16}$$

$$B_{\alpha\beta,\gamma\delta} = -3\lim_{F\to 0}\frac{\partial}{\partial F_{\gamma\delta}}\frac{\partial}{\partial F_\alpha}\frac{\partial}{\partial F_\beta}E^{(1)} = 3\lim_{F\to 0}\frac{\partial}{\partial F_{\gamma\delta}}\frac{\partial}{\partial F_\beta}\mu_\alpha, \tag{17}$$

$$C_{\alpha\beta,\gamma\delta} = -3\lim_{F\to 0}\frac{\partial}{\partial F_{\gamma\delta}}\frac{\partial}{\partial F_{\alpha\beta}}E^{(1)} = \lim_{F\to 0}\frac{\partial}{\partial F_{\gamma\delta}}\Theta_{\alpha\beta}, \tag{18}$$

where we have used $\frac{\partial}{\partial F_\alpha}E^{(1)} = -\mu_\alpha$ and $\frac{\partial}{\partial F_{\alpha\beta}}E^{(1)} = -\frac{1}{3}\Theta_{\alpha\beta}$.

Equations (16)–(18) already give away how the field-free estimators can be derived in the density-matrix picture. Using Eq. (14) as the Hamiltonian, the perturbations $\lambda_1 = F_{\alpha\beta}$ and $\lambda_2 = F_\beta$ yield

$$\begin{aligned} -\frac{\partial\hat{H}}{\partial F_{\alpha\beta}} &= \frac{1}{3}\hat{\Theta}_{\alpha\beta} + \mathcal{O}(F), \\ -\frac{\partial\hat{H}}{\partial F_\alpha} &= \hat{\mu}_\alpha + \mathcal{O}(F), \end{aligned}$$

where $\mathcal{O}(F)$ refers to higher-order terms that vanish as $F \to 0$. Based on Eqs. (7), (9), and (13), A is now given by

$$\begin{aligned} A_{\alpha,\beta\gamma} &= 3\lim_{F\to 0}\frac{\partial}{\partial F_{\beta\gamma}}\langle\mu_\alpha\rangle \\ &= 3\left[\left\langle\mu_\alpha\frac{\partial\rho}{\partial F_{\beta\gamma}}\right\rangle - \langle\mu_\alpha\rangle\left\langle\frac{\partial\rho}{\partial F_{\beta\gamma}}\right\rangle\right] \\ &= \beta\left[\langle\bar{\mu}_\alpha\bar{\Theta}_{\beta\gamma}\rangle - \langle\bar{\mu}_\alpha\rangle\langle\bar{\Theta}_{\beta\gamma}\rangle\right]. \end{aligned} \tag{19}$$

Similarly, we get

$$\begin{aligned} C_{\alpha\beta,\gamma\delta} &= \lim_{F\to 0}\frac{\partial}{\partial F_{\gamma\delta}}\langle\Theta_{\alpha\beta}\rangle \\ &= \frac{\beta}{3}\left[\langle\bar{\Theta}_{\alpha\beta}\bar{\Theta}_{\gamma\delta}\rangle - \langle\bar{\Theta}_{\alpha\beta}\rangle\langle\bar{\Theta}_{\gamma\delta}\rangle\right]. \end{aligned} \tag{20}$$

Finally, using Eq. (8), we can write B as

$$\begin{aligned} B_{\alpha\beta,\gamma\delta} &= 3\lim_{F\to 0}\frac{\partial}{\partial F_{\gamma\delta}}\frac{\partial}{\partial F_\beta}\langle\mu_\alpha\rangle \\ &= \beta^2\left[\langle\bar{\Theta}_{\gamma\delta}\bar{\mu}_\alpha\bar{\mu}_\beta\rangle - \langle\bar{\Theta}_{\gamma\delta}\rangle\langle\bar{\mu}_\alpha\bar{\mu}_\beta\rangle + 2\langle\bar{\Theta}_{\gamma\delta}\rangle\langle\bar{\mu}_\alpha\rangle\langle\bar{\mu}_\beta\rangle\right. \\ &\quad \left. - \langle\bar{\Theta}_{\gamma\delta}\bar{\mu}_\alpha\rangle\langle\bar{\mu}_\beta\rangle - \langle\bar{\Theta}_{\gamma\delta}\bar{\mu}_\beta\rangle\langle\bar{\mu}_\alpha\rangle\right]. \end{aligned} \tag{21}$$

We stress that bar denotes the average over a sample path. Besides that, the implementation of Eqs. (19)–(21) is very straightforward because β is a chosen parameter and $\hat{\mu}_\alpha$ and $\hat{\Theta}_{\alpha\beta}$ are diagonal observables.

III. METHOD

Our method of choice is the path-integral Monte Carlo (PIMC), where the density matrix ρ of N distinguishable particles is obtained by stochastic sampling. In general, we cannot express $\rho(R, R; \beta)$ analytically. Instead, we need to use a discrete path as defined in Eq. (10), which allows us to decompose the full many-body Hamiltonian accurately at a reasonably small time step $\tau = \beta/M$. The method is very accurate, when the finite time step is chosen small enough to eliminate many-body errors. However, this also implies either large path-size M or high temperature, and thus, probing of the low temperature regime is computationally more demanding. In fact, proper integration over the M dimensions of dR_i is a formidable task at any discretization. Thus, it is necessary to use Metropolis sampling and other advanced algorithms for efficient Monte Carlo integration. This involves nothing out of the ordinary from an implementation of PIMC, and thus, we shall direct a curious reader to more dedicated resources, e.g., Refs. 10 and 11.

The convenience of the Metropolis algorithm also emerges in the sampling of any spatial degrees of freedom, including the rovibrational motion of the nuclei. In particular, we can easily differentiate between adiabatic and non-adiabatic simulations. We will refer to these as Born–Oppenheimer (BO) and all-quantum (AQ), respectively. In BO simulation, the nuclei are fixed in space, whereas in AQ simulation they are free to move confined only by the implicit interaction of the electronic bonding. The resulting nuclear motion yields the correct rovibrational sampling, including the zero-point motion.[12] Likewise, the simulation of positrons is only a matter of choosing the charge and mass because full explicit correlation is already included in the density matrix.

However, the situation is more complicated for identical particles, especially Fermions. In simulations involving the exchange interaction, a numerical sign problem arises from the antisymmetry. Various schemes have been developed to approach the Fermion sign problem (e.g., Ref. 13), but they will likely have implications on the polarizability estimators proposed in this work. Therefore, we will leave that as a subject for another study and only concentrate on the simulation of up to two Fermions (effectively, electrons or positrons), whose spin states we can safely sample using the Boltzmann statistics.

IV. RESULTS

We demonstrate the finite temperature computation of the field-gradient polarizabilities with our path-integral Monte Carlo code and the estimators based on Eqs. (19)–(21). The simulations are exact apart from a small time step error from the many-body correlations. At longer time steps τ, extrapolating $\tau \to 0$ helps us to improve the result and provide upper bound estimates for properties that are converging from below and vice versa. However, in the adiabatic simulation with the Boltzmann statistics, the error is most effectively eliminated by simply using a reasonably small τ. In the following adiabatic (BO) simulations, we shall use $\tau = 0.025$ for H and Ps systems, $\tau = 0.006\,25$ for He and Li systems, and $\tau = 0.003\,125$ for Be^{2+}. The non-adiabatic (AQ) results have been extrapolated linearly to $\tau \to 0$, using $\tau = 0.025$, 0.0125 for HeH^+ and $\tau = 0.05$, 0.025 otherwise. The statistical error estimate is given by standard error of the mean (SEM) with 2σ, i.e., 2SEM. All results are given in atomic units.

In the following, we present polarizability data and discussion for a variety of isolated one or two-electron systems: H, H^-, Li^+, Be^{2+}, H_2^+, H_2, PsH, Ps_2, H_3^+, and HeH^+. We run two kinds of simulations: adiabatic and non-adiabatic. In the adiabatic or Born–Oppenheimer approximation (BO), the nuclei are fixed in space, reducing symmetry and producing various directional components to polarizabilities. The adiabatic approximation inhibits the rovibrational motion, and thus, at reasonably low temperatures, the difference to absolute zero is negligible. Therefore, we start by establishing the validity of our method by comparing our BO results to the available 0 K reference data.

An excellent summary of independent tensorial polarizabilities for each point group is given in Ref. 1. In Table I, we present BO results for all of the spherically symmetric systems: $B_{zz,zz}$, $C_{zz,zz}$ and the total energy E. Furthermore, the results for the molecular systems, i.e., H_2^+, H_2 H_3^+, and HeH^+, are given in Table II. Each molecular system has one independent quadrupole moment Θ_{zz} and four independent dipole–dipole–quadrupole polarizabilities: $B_{zz,zz}$, $B_{xx,xx}$, $B_{zz,xx}$, and $B_{xz,xz}$. Similarly, there are three independent components

TABLE I. Total energies E, dipole–dipole–quadrupole polarizabilities B, and quadrupole–quadrupole polarizabilities C of spherically symmetric systems, matched with suitable literature references. All results in atomic units.

	E	$B_{zz,zz}$	$C_{zz,zz}$
H	−0.49995(3)[a]	−106.5(3)[a]	5.003(4)[a]
	−0.5	−106.5[b]	5.0[b]
H^-	−0.52766(10)[a]	$-4.78(87) \times 10^5$[a]	2568(136)[a]
	−0.527 75[c]	-4.843×10^5[d]	2591.6[d]
He	−2.9037(2)[a]	−7.32(9)[a]	0.814(2)[a]
	−2.90372[c]	−7.326 7[e]	0.815 0[e]
Li^+	−7.2800(7)[a]	−0.121(3)[a]	0.037 97(9)[a]
	−7.279913[f]	−0.121 4[e]	0.037 96[e]
Be^{2+}	−13.6547(12)[a]	−0.008 3(3)[a]	0.005 106(15)[a]
	−13.655566[f]	−0.008 393[e]	0.005 106 7[e]
PsH	−0.7893(3)[a]	5300(260)[a]	260(3)[a]
	−0.789 13[g]		
Ps_2	−0.515 97(7)[a]	0(440)[h]	460(7)[a]
	−0.516 003 8[i]		

[a]This work.
[b]Bishop and Pipin.[14]
[c]Nakashima and Nakatsuji.[15]
[d]Pipin and Bishop.[27]
[e]Bishop and Rérat.[16]
[f]Johnson and Cheng.[17]
[g]Frolov and Smith.[28]
[h]This work; estimating anything other than 0 is unfeasible because of the large fluctuations.
[i]Bubin *et al.*[29]

TABLE II. Total energies E, independent quadrupole moments Θ, dipole–dipole–quadrupole polarizabilities B, and quadrupole–quadrupole polarizabilities C of molecular systems at fixed orientation, matched with suitable literature references. All results in atomic units.

	E	Θ_{zz}	$B_{zz,zz}$	$B_{xx,xx}$	$B_{xx,zz}$	$B_{xz,xz}$	$C_{zz,zz}$	$C_{xx,xx}$	$C_{xz,xz}$
H_2^+	−0.602 7(2)[a]	1.530 71(8)[a]	−41.9(9)[a]	−13.24(14)[a]	7.3(3)[a]	−18.10(4)[a]	1.913(12)[a]	1.268(5)[a]	1.1946(7)[a]
	−0.602 634[b]	1.530 7[c]	−41.869[d]	−13.249[d]	7.3052[d]	−18.099[d]	1.9113[d]	1.2670[d]	1.1945[d]
H_2	−1.174 6(4)[a]	0.456 3(2)[a]	−90.7(10)[a]	−66.8(8)[a]	34.5(10)[a]	−58.7(3)[a]	5.99(2)[a]	4.930(13)[a]	4.176(6)[a]
	−1.174 474[e]	0.456 84[f]	−90.29[g]	−66.83[g]	34.37[g]	−59.00[g]	5.983[g]	4.927[g]	4.180[g]
H_3^+	−1.344 0(4)[a]	−0.919 53(10)[a]	−11.7(3)[a]	−19.0(2)[a]	9.1(4)[a]	−11.07(4)[a]	1.557(10)[a]	2.078(6)[a]	1.2441(10)[a]
	−1.343 835 6[h]								
	−1.335 18[i]	−0.926 13[i]							
HeH^+	−2.978(2)[a]	1.249 56(13)[a]	−5(8)[a]	−2.07(12)[a]	1.0(3)[a]	−2.25(9)[a]	0.59(2)[a]	0.396(6)[a]	0.3382(5)[a]
	−2.978 706[j]								

[a]This work.
[b]Turbiner and Olivares-Pilon.[18]
[c]Bates and Poots.[19]
[d]Bishop and Cheung.[20]
[e]Kolos and Wolniewicz.[21]
[f]Poll and Wolniewicz.[22]
[g]Bishop *et al.*[23]
[h]Turbiner and Lopez Vieyra.[25]
[i]Carney and Porter.[24] ($R = 1.6504$).
[j]Pachucki.[26]

of quadrupole–quadrupole polarizabilities: $C_{zz,zz}$, $C_{xx,xx}$, and $C_{xz,xz}$. Distinct symmetries also lead to a few non-zero dipole–quadrupole polarizabilities A: for H_3^+, $A_{y,yy} = -0.653(7)$ and for HeH^+ $A_{z,zz} = -0.48(4)$ and $A_{x,zx} = -0.0660(9)$. The principal axis z is by default the line connecting the two nuclei, but for triangular H_3^+, it is perpendicular to the plane of protons. In BO simulation, the molecules are placed at the equilibrium geometries, namely, $R_{H_2^+} = 2.0$, $R_{H_2} = 1.4$, $R_{H_3^+} = 1.65$, and $R_{HeH^+} = 1.46$. The dipole and quadrupole moments are calculated with respect to the center-of-mass. By default, the temperature is set to $T = 2000$ K, which still corresponds to the electronic ground state for most systems. However, to be certain, we use $T = 1000$ K for H_2, $T = 500$ K for PsH, and $T = 100$ K for H^- and Ps_2. The data for positronium, Ps, are missing because the symmetry of masses $m_{\bar{e}} = m_e$ makes its quadrupole moment vanish. The largest discrepancy is in Θ_{zz} of H_3^+: based on our calculations and the reference energy, the cause is more likely in the basis functions of Ref. 24 than in the effects of temperature, time step, or equilibrium distance. Otherwise, the agreement is good with most of the available 0 K literature Refs. 14–26. Many properties of the molecular ions and the positron systems are also reported for the first time.

To non-adiabatic simulations, we refer as *all-quantum* (AQ) since they include all rovibrational and electronic quantum effects. Switching off the adiabatic approximation is simple: the nuclei are simulated and allowed to move like electrons, only with bigger mass. For atoms, the difference is negligible, but in molecules, this arouses considerable thermal coupling of properties, such as the polarizabilities. We use $m_p = 1836.152\,672\,48 m_e$ for proton mass and $m_{He} = 7294.299\,536\,3 m_e$ for that of He-nucleus. The AQ simulations are done in the laboratory coordinates, which is denoted by capital Z. The results are exact rovibrationally averaged quantities and therefore spherically symmetric. Consequently, $A_{Z,ZZ}$ are zero for all systems. The resulting temperature-dependent data for $B_{ZZ,ZZ}$ and $C_{ZZ,ZZ}$ for H_2^+, H_2, H_3^+, and HeH^+ are presented in Fig. 1 in order to show that any time step effects are negligible. The actual numerical and extrapolated data can be found in the supplementary material.

Any non-zero electric moments of a quantum system couple to its rotational states, and then this coupling is manifested in the rotational parts of higher order polarizabilities. At high temperatures, this rotational coupling is proportional to the inverse temperature, which has already been proposed[4,34] and demonstrated.[5] Now, for homonuclear molecules, H_2^+, H_2, H_3^+, the first non-zero electric moment is the quadrupole moment Θ, and thus, all of these systems show $\sim 1/T$ decay on B and C. For HeH^+ with non-zero dipole moment μ, the dipole polarizability α is also affected by the coupling.[5] Thus, it makes sense that B of HeH^+, involving both α and Θ, is in fact proportional to $\sim 1/T^2$.

However, the rotational polarizabilities do not diverge at low temperatures because it takes some energy to activate the rotational states. To model the temperature dependence of the total B and C, we propose an *ad hoc* nonlinear function of the form

$$f(T) = \left(\frac{a_1 \cdot \mathrm{erf}(a_2 T)}{T} \right)^x + a_3, \tag{22}$$

where a_1, a_2, and a_3 are coefficients and the error function $\mathrm{erf}(y)$ is used to saturate the values in a robust way as $T \to 0$. As argued earlier, a natural choice for the characteristic exponent describing the rotational coupling is $x = 1$ ($x = 2$ for B of HeH^+). However, we also present x optimized by the root-mean-squared error (RMSE) as a crude means of considering nontrivial thermal effects originating from the electronic and vibrational polarizabilities. Nonlinear fitting to time step extrapolated data has been done using fitnlm function in Matlab, which also provides 95% confidence intervals. Inversed squares of SEM estimates of the PIMC data were used as weights.

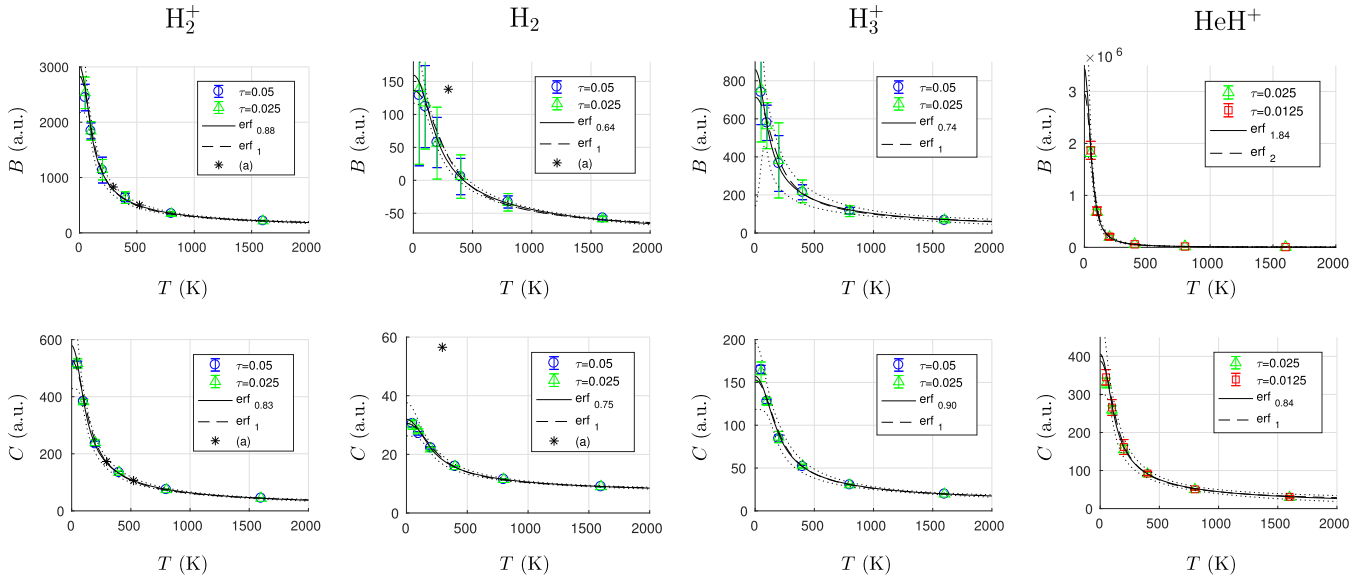

FIG. 1. Rovibrationally averaged dipole–dipole–quadrupole polarizabilities $B_{ZZ,ZZ}$ and quadrupole–quadrupole polarizabilities $C_{ZZ,ZZ}$ for nonadiabatic simulations of molecular systems plotted at different temperatures. A few data points from Ref. 34 have been marked with (a). Fits to Eq. (22) are presented with solid line for optimal exponent x and dashed line for integer exponent. Dotted lines are 95% confidence boundaries given by the fitting algorithm.

TABLE III. Total energies, dipole–dipole–quadrupole polarizabilities, and quadrupole–quadrupole polarizabilities extrapolated to 0 K. Quadratic fit is used for E, and Eq. (22) with optimal x for B and C. All results in atomic units.

	E	$B_{ZZ,ZZ}$	$C_{ZZ,ZZ}$
H_2^+	−0.596(2)[a]	3000(850)[a]	580(150)[a]
	−0.597 139[b]		
H_2	−1.162 5(11)[a]	160(35)[a]	32(6)[a]
	−1.164 025[c]		
H_3^+	−1.323(5)[a]	860(720)[a]	157(39)[a]
	−1.323 568[d]		
HeH^+	−2.967 0(8)[a]	$3.4(1.7) \times 10^6$[a]	406(110)[a]
	−2.966 27[e]		

[a]This work (extrapolated to 0 K).
[b]Tang *et al.*[30]
[c]Stanke *et al.*[31]
[d]Kylänpää and Rantala.[32]
[e]Calculated based on Refs. 26 and 33.

Extrapolation of Eq. (22) to $T = 0$ is given by $\frac{2}{\sqrt{\pi}} a_1 a_2 + a_3$. The corresponding data for B and C are presented in Table III together with quadratically extrapolated total energies and appropriate Refs. 26 and 30–33. The raw data and the fitting coefficients can be found in the supplementary material. Besides Fig. 1, the fitted curves are presented on a logarithmic scale in Fig. 2. It is easier to see that the rotational polarizability is saturated at low T but decays as T^{-x} as the rotational states get activated. Also, it can be observed that the magnitudes of the rotational parts of B (except for HeH^+) and C are clearly in the same order as the corresponding lower order moments, Θ_{zz}, from Table II.

The high-temperature limit of the fit is given by a_3. It gives the ballpark of the sum of the vibrational and electronic polarizabilities, whose thermal coupling is much smaller but not negligible. This is manifested in the characteristic exponent x: the optimal x in a least-squares fit appears to be slightly smaller than a natural integer, 1 or 2. While the exponent in T^{-x} is probably not the most natural way to model this, it shows evidence on how the vibrational and electronic parts compensate on the decay of rotational polarizability. Furthermore, to first approximation, the electronic part of AQ polarizability should equal to the isotropic average (see Ref. 4) of the BO values. One delusive example would be correlating the isotropic average $\langle B \rangle_{ZZ,ZZ} = -74.65$ of H_2 to its high-temperature limit, −82.828. Unfortunately, a quick survey reveals that the high-temperature limit seldom agrees with the averaged electronic quantities from 0 K. This underlines the difficulty of decomposing the dielectric properties under strong thermal influence, and we attempt to do it no further.

As a final remark, we discuss the only explicit reference for the finite temperature total polarizabilities given by Bishop and Lam.[34] As shown in Fig. 1, their results are a good match for H_2^+ but severely overestimated for H_2. We suggest that this is caused by inaccuracy of the vibrational wave function basis used by the authors. Due to the electronic correlations, their ground state is not exact but rather an uncontrollable mixture involving higher excited vibrational eigenstates. According to their own tables, such vibrational bias leads to unintended overestimation of properties, which can be substantial in case of polarizabilities. This example discloses the inherent sensitivity of estimating higher order electric properties in many-body systems.

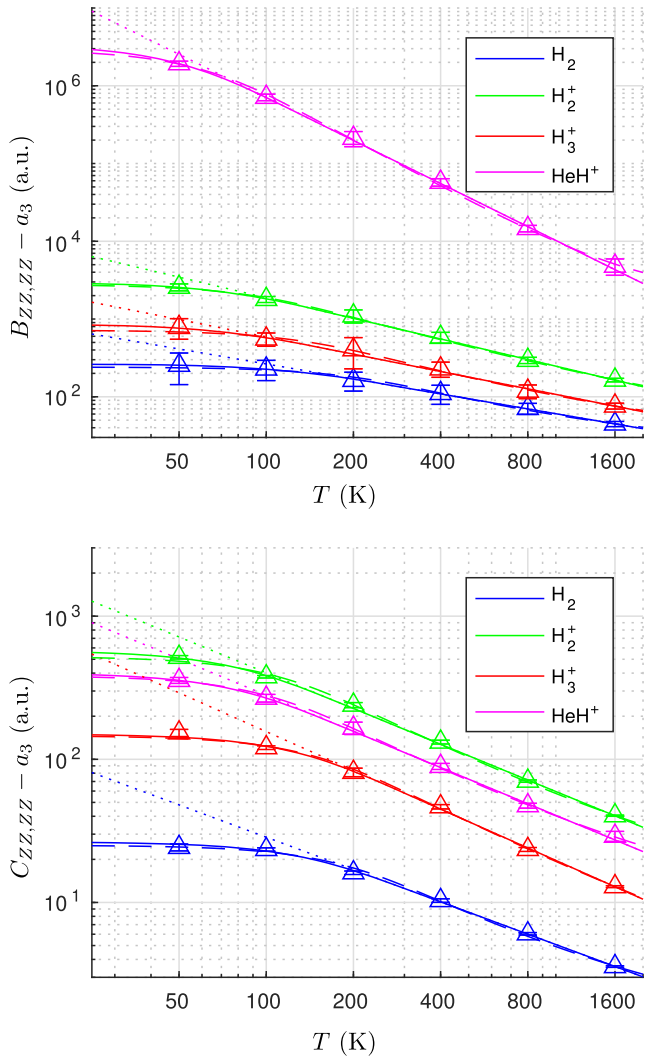

FIG. 2. Time step extrapolated data and nonlinear fits for B and C of H_2^+, H_2, H_3^+, and HeH^+ on a logarithmic scale. The fits to Eq. (22) are done with $x = 1$ (dashed) or the optimal x (solid). Dotted lines show the effect of replacing the error function with unity.

V. SUMMARY

As a natural continuation to our previous work, we present a scheme to estimate static field-gradient polarizabilities in a field-free PIMC simulation. We apply it on a range of small atoms, ions, and molecules, namely, H, H^-, He, Li^+, Be^{2+}, Ps_2, PsH, H_2^+, H_2, H_3^+, and HeH^+. The simulations with the adiabatic approximation and equilibrium geometries are done in the low temperature limit, and they indeed agree well with the 0 K literature references. However, we do not try to push the limits of statistical precision in this study, but rather, we want to give an ample demonstration of our method.

With the given set of systems, the variation in dielectric properties is already large. For instance, H^- or PsH are very diffuse compared to the heavier ions, Li^+ and Be^{2+}. On the

other hand, HeH^+ has a permanent dipole moment and thus much more diverse dielectric response than the homonuclear molecules. We want to emphasize that all these properties were obtained with the same PIMC procedure varying nothing else than the fundamental properties of the particles.

One of the most advantageous treats of the PIMC method is the exact simulation of the canonical ensemble. Molecules have geometrical anisotropy and thus permanent dipole or quadrupole moments, which then reflect in the higher order rotational polarizabilities. Our data indicate that the rotational parts of $B_{ZZ,ZZ}$ and $C_{ZZ,ZZ}$ are dominant at low temperatures but decay drastically when the temperature is increased. The latter effect has been anticipated in the literature,[4] but even our overly simplistic model in Eq. (22) shows that there is plenty of room for improvement. Indeed, the requirements of explicit correlations and non-adiabatic thermal averaging render results of this kind very scarce. By this work, we are hoping to inspire a change to that.

SUPPLEMENTARY MATERIAL

See supplementary material for the raw data of non-adiabatic PIMC simulations and the non-linear fitting.

ACKNOWLEDGMENTS

We thank Jenny and Antti Wihuri Foundation and Tampere University of Technology for financial support. Also, we acknowledge CSC–IT Center for Science Ltd. and Tampere Center for Scientific Computing for providing us with computational resources.

[1] A. D. Buckingham, *Permanent and Induced Molecular Moments and Long-Range Intermolecular Forces* (John Wiley & Sons, Inc., 2007), pp. 107–142.
[2] G. Maroulis, *Computational Aspects of Electric Polarizability Calculations: Atoms, Molecules and Clusters* (IOS Press, 2006).
[3] J. Mitroy, M. S. Safronova, and C. W. Clark, J. Phys. B: At., Mol. Opt. Phys. **43**, 202001 (2010).
[4] D. M. Bishop, Rev. Mod. Phys. **62**, 343 (1990).
[5] J. Tiihonen, I. Kylänpää, and T. T. Rantala, Phys. Rev. A **94**, 032515 (2016).
[6] J. Tiihonen, I. Kylänpää, and T. T. Rantala, Phys. Rev. A **91**, 062503 (2015).
[7] I. Leontyev and A. Stuchebrukhov, Phys. Chem. Chem. Phys. **13**, 2613 (2011).
[8] C. M. Baker, Wiley Interdiscip. Rev.: Comput. Mol. Sci. **5**, 241 (2015).
[9] J. Tao and A. M. Rappe, J. Chem. Phys. **144**, 031102 (2016).
[10] D. M. Ceperley, Rev. Mod. Phys. **67**, 279 (1995).
[11] I. Kylänpää, "First-principles finite temperature electronic structure of some small molecules," Ph.D. thesis, Tampere University of Technology, 2011.
[12] I. Kylänpää, M. Leino, and T. T. Rantala, Phys. Rev. A **76**, 052508 (2007).
[13] W. R. Magro, B. Militzer, D. M. Ceperley, B. Bernu, and C. Pierleoni, "Restricted Path Integral Monte Carlo Calculations of Hot, Dense Hydrogen," in *Strongly Coupled Coulomb Systems* (Springer, 2002), pp. 337–340.
[14] D. M. Bishop and J. Pipin, Chem. Phys. Lett. **236**, 15 (1995).
[15] H. Nakashima and H. Nakatsuji, J. Chem. Phys. **127**, 224104 (2007).
[16] D. M. Bishop and M. Rérat, J. Chem. Phys. **91**, 5489 (1989).
[17] W. R. Johnson and K. T. Cheng, Phys. Rev. A **53**, 1375 (1996).
[18] A. V. Turbiner and H. Olivares-Pilon, J. Phys. B: At., Mol. Opt. Phys. **44**, 101002 (2011).
[19] D. R. Bates and G. Poots, Proc. Phys. Soc. A **66**, 784 (1953).
[20] D. M. Bishop and L. M. Cheung, J. Phys. B: At., Mol. Opt. Phys. **12**, 3135 (1979).
[21] W. Kolos and L. Wolniewicz, J. Chem. Phys. **49**, 404 (1968).
[22] J. D. Poll and L. Wolniewicz, J. Chem. Phys. **68**, 3053 (1978).
[23] D. M. Bishop, J. Pipin, and S. M. Cybulski, Phys. Rev. A **43**, 4845 (1991).
[24] G. D. Carney and R. N. Porter, J. Chem. Phys. **60**, 4251 (1974).
[25] A. V. Turbiner and J. C. Lopez Vieyra, J. Phys. Chem. A **117**, 10119 (2013).
[26] K. Pachucki, Phys. Rev. A **85**, 042511 (2012).
[27] J. Pipin and D. M. Bishop, J. Phys. B: At., Mol. Opt. Phys. **25**, 17 (1992).
[28] A. M. Frolov and V. H. Smith, Phys. Rev. A **56**, 2417 (1997).
[29] S. Bubin, M. Stanke, D. Kędziera, and L. Adamowicz, Phys. Rev. A **75**, 062504 (2007).
[30] L.-Y. Tang, Z.-C. Yan, T.-Y. Shi, and J. F. Babb, Phys. Rev. A **90**, 012524 (2014).
[31] M. Stanke, D. Kçedziera, S. Bubin, M. Molski, and L. Adamowicz, J. Chem. Phys. **128**, 114313 (2008).
[32] I. Kylänpää and T. T. Rantala, J. Chem. Phys. **133**, 044312 (2010).
[33] W.-C. Tung, M. Pavanello, and L. Adamowicz, J. Chem. Phys. **137**, 164305 (2012).
[34] D. M. Bishop and B. Lam, Chem. Phys. Lett. **143**, 515 (1988).